

Dual-Detector Probe for Surgical Tumor Staging

T. S. Hickernell, H. B. Barber, H. H. Barrett, and J. M. Woolfenden

Optical Sciences Center and Department of Radiology, University of Arizona, Tucson, Arizona

A hand-held, dual-detector probe has been developed for surgical tumor staging. This dual probe simultaneously monitors counts from a possible tumor site along with counts from adjacent normal tissue using two concentric, collimated scintillation detectors. A comparison of counts from the detectors can distinguish a small tumor directly in front of the probe from variations in background activity. The probe was tested in computer simulations of surgical staging of metastases to para-aortic and iliac lymph nodes using a spatial response map of the probe, a numerical torso phantom, and organ activity data for [⁵⁷Co]bleomycin in rabbits. Results show that the dual probe performs better than a single-detector probe in detecting tumors and solves the problem caused by spatial variations in the background source distribution.

J Nucl Med 29:1101-1106, 1988

External imaging has had poor success in localizing soft-tissue tumors smaller than 2 cm in diameter, particularly when they are located deep in tissue (1,2). Problems include the low sensitivity of gamma imaging systems and low tumor uptake of the radiopharmaceutical. Tumor activity for existing soft-tissue tumor markers is rarely greater than a few hundred nCi per cubic centimeter. With camera collimator efficiencies on the order of 10^{-4} , rates from small tumors ($<1 \text{ cm}^3$) are $<1 \text{ c/sec}$ at the detector. Attenuation and scatter in tissue further reduce count rates for deep tumors. Moreover, target-to-nontarget uptake ratios for existing pharmaceuticals are rarely greater than 10:1 (2-4) so that uptake in normal tissue presents a substantial background.

Detection sensitivity can be improved by moving a detector close to the tumor. This decreases the attenuating and scattering tissue between the source and detector and increases the solid angle subtended by the source at the detector. Small scintillation and semiconductor probes have been constructed for insertion into the body for tumor detection during bronchoscopy or surgery (1-3,5,6). Such probes have detected tumors of diameter $<1 \text{ cm}$.

However, detection procedures that use probes have difficulty distinguishing activity variations near the

probe, such as those due to tumors, from background activity variations that arise from different uptakes of the radiopharmaceutical in different normal tissues (1,5,7). Thus an increase in count rate as the probe is moved may arise from a tumor near the detector or from the change of the detector position or orientation with respect to a distant organ of high activity. Diagnostic error may result and, for this reason, the advantages of probes are often not fully realized in practice.

In this paper we report the design and testing of a new probe, the "dual probe." It is designed with two concentric detectors to solve the problems caused by spatial variations in the background. A dual-probe system with concentric detectors was employed by Groch et al. (8) for a different task, the measurement of left ventricular ejection fraction. Our dual probe was tested in computer simulations of surgical staging using a numerical torso phantom. Its performance was assessed using instrumental receiver operating characteristic (ROC) analysis and compared to the performance of a single-detector probe.

MATERIALS AND METHODS

Design of the Dual Probe

The dual probe was designed with two independent NaI(Tl) scintillation detectors: a central, or inner, detector and a concentric outer detector (Fig. 1). Both detectors view the same background distribution, but the inner detector is substantially more sensitive to a small volume directly in front of the probe. Thus a comparison of counts from the detectors

Received Sept. 3, 1987; revision accepted Dec. 22, 1987

For reprints contact: James M. Woolfenden, MD, Div. of Nuclear Medicine, Arizona Health Sciences Center, Tucson, AZ 85724.

can disclose increased activity, such as a tumor, in this sensitive region. In the Appendix we discuss a suitable comparison of counts.

Several designs of the dual probe were considered, differing in their collimator geometries and detector radii. For each design we made radiometric calculations of the probe's response to various tumors in a uniform background source. Tumors ranged from 0.5 to 1.0 cm in diameter and had an activity of 24 nCi per cm³. The background was modeled by a spatially uniform source 5 cm thick with an activity of 2.4 nCi per cm³. We calculated the ROC figure of merit d_a (see Appendix) for each design and used these values to compare designs.

These calculations gave two interesting results. First, for the probe in contact with a tumor of fixed size, there is an inner detector diameter that maximizes d_a . Figure 2 shows, not surprisingly, that this optimum diameter is approximately equal to the diameter of the tumor presented. The second result is shown in Figure 3. The probe's sensitivity to tumors located near the probe face is greatest for short collimator lengths. For deeper tumors, longer collimators are best. Superficial tumors subtend large solid angles at the inner detector. Short collimators help maximize the sensitivity to these tumors by allowing a large inner-detector field of view. Deeper tumors subtend smaller solid angles and overlap the field of view of the outer detector. Thus the probe views part of the tumor as a background source. Longer collimators restrict the field of view of the inner detector so that it is less sensitive to background sources and restricts the field of view of the outer detector so it is less sensitive to the tumor. In effect, longer collimators extend the sensitive region of the probe. The optimum probe design, therefore, depends on both the size and the depth of the tumors expected.

The dual probe was designed primarily for surgical staging of lymph node metastases in the abdomen and pelvis. This task is particularly well suited to the probe because a limited number of nodes must be searched, and the probe can usually be placed in contact with each node. A photograph of this probe is shown in Figure 4. The inner detector is 0.6 cm in diameter, consistent with the small (<1 cm) size expected for lymph nodes harboring occult metastases. The outer detector has an outer diameter of 1.8 cm and an area five times the

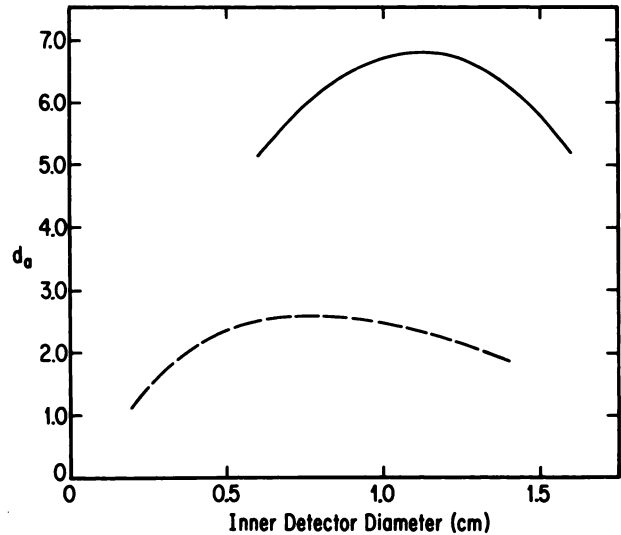


FIGURE 2
Plot of d_a versus inner detector diameter for 1.0 cm diameter tumor (solid) and 0.5 cm diameter tumor (dashed). Tumors are located in contact with probe directly in front of inner detector. Diameter of probe (2.54 cm) and thickness of inner collimator (0.25 cm) are held constant.

area of the inner detector. Because the probe is to be used in contact with suspected tumors, the collimators extend only 0.5 mm beyond the faces of the detectors. The two NaI(Tl) scintillators are 0.6 cm long and are separated by a 0.1-cm-thick lead collimator. This assembly is housed in a hermetically sealed aluminum container. The crystals are coupled to photomultiplier tubes by separate fiberoptic light guides contained in a common flexible sheath. A chain of event electronics, including a preamplifier, amplifier, single channel analyzer, and counter, follows each photomultiplier tube. The counters are on accessory boards in a personal computer which provides on-line data acquisition, analysis, and display. The electronics (not shown in Fig. 4) are completely portable, incorporated within a half-size NIM bin and the personal computer.

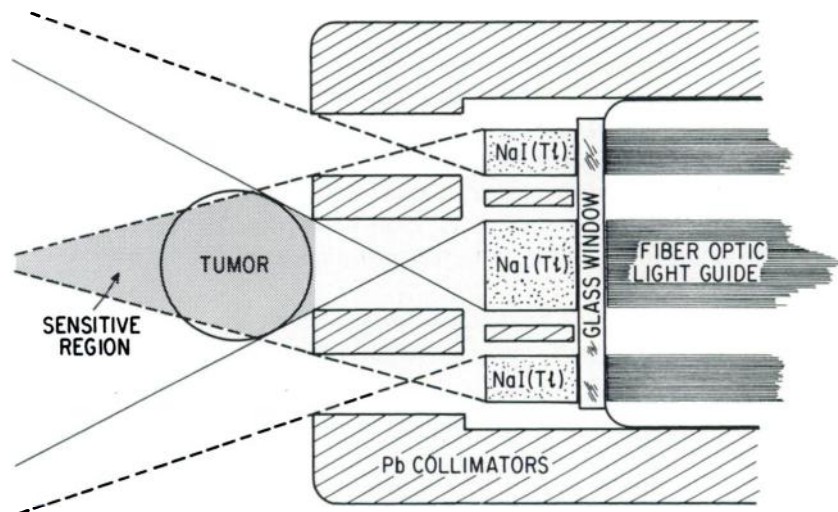


FIGURE 1
Cross-sectional schematic of dual probe. Collimator design produces sensitive region directly in front of inner detector. Geometry is rotationally symmetric.

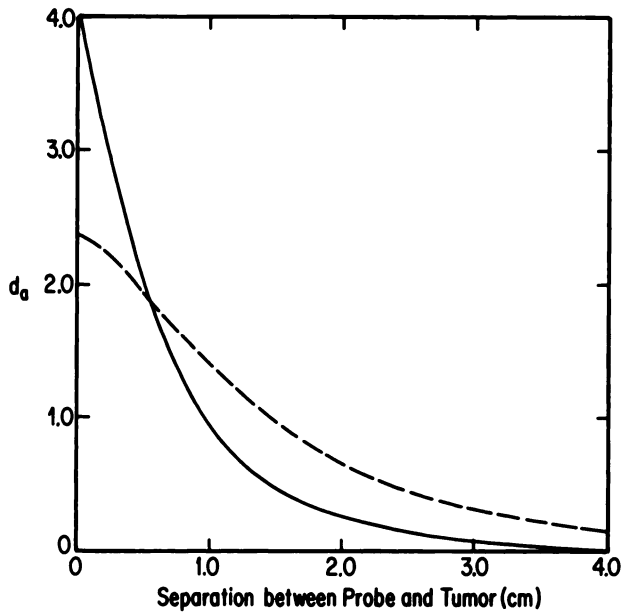


FIGURE 3
Plot of d_0 versus separation of probe and tumor for 0.2 cm collimator (solid) and 0.6 cm collimator (dashed).

RESULTS AND DISCUSSION

Spatial Response of the Probe

We mapped the point-response function of the probe using a small source of ^{57}Co . Count rates in both detectors were recorded for each placement of the source in a plane containing the axis of rotational symmetry of the probe. These measurements and the assumption of rotational symmetry gave a spatial map of the probe response from which its total response to any activity distribution could be calculated. The mapping procedure was carried out with the probe and sources inside a water tank to include effects of attenuation and Compton scatter. The tank was approximately the size of a human torso (30 cm \times 30 cm \times 50 cm).

Figure 5 shows the results of the count rate measurements presented as a spatial "differential sensitivity" map in an axial plane of the probe. We define differential sensitivity by $r_i - Fr_o$, where r_i and r_o are count rates in the inner and outer detectors, respectively, that result from a point source of unit activity. The normalization constant F is described in the Appendix. For the map in Figure 5 we used $F = 0.27$. A region of high sensitivity is indicated near the probe face. All source points in this region contribute substantially more to the count rate in the inner detector, r_i , than to the normalized count rate in the outer detector, Fr_o . Sources far from the probe contribute to the count rates in the proportion of $r_i \approx Fr_o$. Although these sources present a background to the inner detector, information about their contribution to the background is recorded in the outer detector. A region of negative differential sensitivity is also evident in the map. This occurs near the

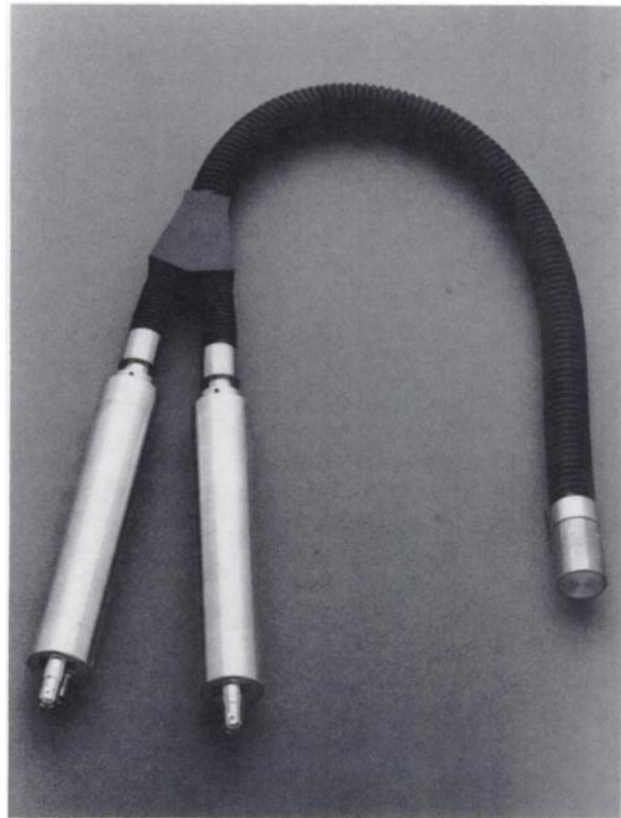


FIGURE 4
Photograph of dual probe showing crystal housing, fiber-optic light guides in black plastic sheath, and two photomultiplier tubes.

edges of the probe where source points contribute substantially more to the count rate in the outer detector. The decrease in the probe's sensitivity due to sources in this region is small compared to the increase in sensitivity for a source in front of the inner detector, so localized spots of high activity near the edges of the probe do not significantly degrade probe performance.

Phantom Construction and Surgical Simulation

We constructed a numerical torso phantom by digitizing transverse slices from an atlas of cross-sectional anatomy. The phantom contains 45,448 voxels, each measuring 1 cm \times 1 cm \times 1.3 cm, and each assigned to one of 19 organs. With a given organ activity distribution for the phantom we can simulate many clinical procedures such as external gamma imaging and endoscopic or surgical tumor detection using probes.

We estimated the distribution and covariation of ^{57}Co bleomycin in human organs using activity distribution data for nine major organs in rabbits. For these estimates we assumed the fractional uptake of the administered dose for an organ to be the same in the rabbit and human. The estimates were used to form a multivariate normal probability law of nine parameters comprising the nine organ activities. Activity variation and covariation were preserved in the probability law. From

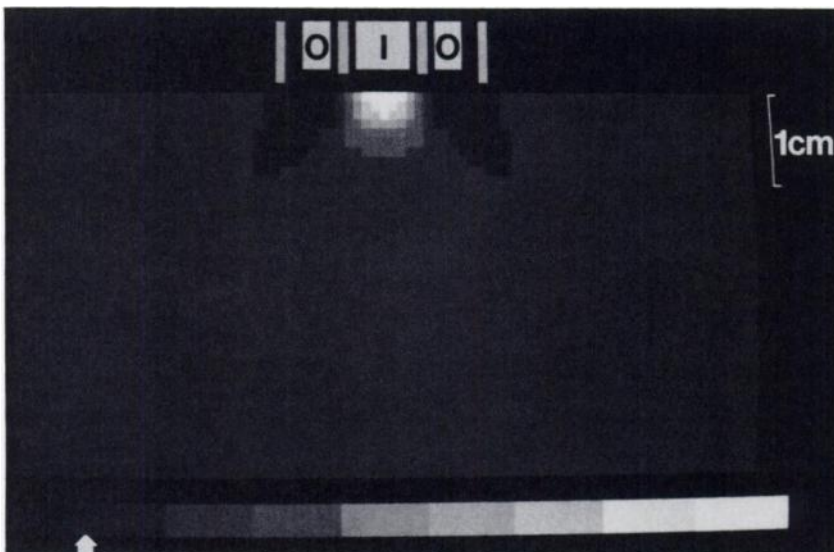


FIGURE 5
Differential sensitivity map in front of dual probe. Cross section of dual probe with inner detector (I) and outer detector (O) separated by collimators is also shown. We have plotted $r_i - Fr_o$ for point source. Arrow indicates grey level corresponding to differential sensitivity of O. Map covers a field 4 cm x 8 cm and is rotationally symmetric.

this law we chose 1,000 sets of organ activities and simulated 1,000 patients. Activities for the 10 organs in the torso phantom that were not represented in the activity distribution data were assigned with the assumption that similar human tissues have similar uptakes of the radiopharmaceutical. For example, we assumed that the intestines and stomach have the same activity per cubic centimeter of tissue.

To simulate metastases, ~7,000 tumors of random activity (1–8 times the average local activity) were distributed among 14 para-aortic and iliac lymph-node sites in the 1,000 patients. These tumors were 1 cm in diameter.

Using the measured point-response maps, the numerical torso phantom, and the activity distribution data, we simulated a surgical tumor staging procedure with the help of a VAX 8600 computer. Count rates for both detectors were computed by summing the count rate contributions of each torso voxel. For each simulated patient we obtained 14 sets of count rates corresponding to the 14 lymph-node sites. Poisson noise corresponding to a specified count time was added to each data set.

Evaluation of Probe Performance

The dual-probe performance in the simulated surgical procedure was evaluated at count times ranging from 0.1 to 1,000 sec. For each count time we calculated the test statistic Λ_d (see Appendix) for all 14,000 sets of counts and divided the data into 100 groups. The area under the receiver operating characteristic (ROC) curve was calculated for each group and from these areas we computed a mean area and standard error. Note that there is no human observer used in this analysis. All ROC-curve areas were calculated directly from the samples of the decision variable, Λ_d .

We also evaluated the performance of a single-detector probe, the inner detector alone, given the same

simulated task as the dual probe. The test used with the single-detector data was

$$\Lambda_s = c_i - b_i,$$

where c_i is the inner detector count and b_i is the local background count in the inner detector. Since c_i and b_i cannot be simultaneously measured at the lymph node in question, the inner detector count at the lymph node nearest the node of interest was used as a measurement of the background count, b_i .

In Figure 6 we have plotted the area under the ROC curve at various count times for the dual- and single-detector probes. For reasonable count times during surgery, ~1 to 10 sec per site, the dual probe performs much better than the single-detector probe. The figure

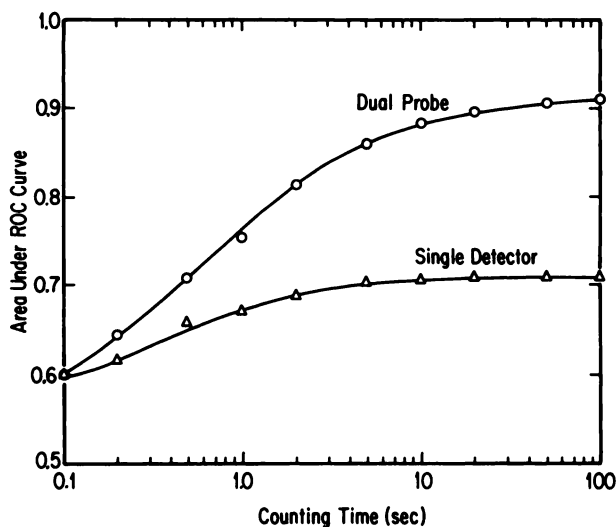


FIGURE 6
Plot of area under ROC curve versus count time for single-detector probe and dual probe. Errors in areas are given by sizes of circles and triangles.

also shows how Poisson noise and background count-rate variations limit system performance. For count times less than 5 sec, both probe systems are limited by Poisson noise so that their performances improve with longer count time. For count times >5 sec the non-uniformity of the background source distribution limits the performance of the single-detector probe so an increase in count time does not improve probe performance. The dual probe is less sensitive to background count rate variations and thus its performance continues to improve with longer count times. Beyond 20 sec the background fluctuations also limit the dual-probe system although the performance level of the dual probe is now much better than the single-detector probe. Figure 6 shows quite clearly that the dual probe is effective in solving the problem caused by fluctuations in the background count rate.

CONCLUSIONS

We have designed and constructed a dual-detector probe for use in surgical tumor staging. It solves the problem presented by spatial variations in the background source distribution. Preliminary measurements and computer simulation results indicate that the dual probe performs much better than a single-detector probe in realistic detection tasks. We used scintillation detectors in our probe but a dual probe built with semiconductor detectors should give similar results. The use of the probe with indium-111-labeled monoclonal antibodies to detect colorectal and prostate cancer is now being investigated.

APPENDIX

When the dual probe is used to determine whether a region of interest contains a tumor, we receive count data, c_i and c_o , from the inner and outer detectors, respectively. Using these data we must decide whether a tumor is present. This Appendix describes the features of a suitable test for tumor presence and a figure of merit to evaluate probe performance.

An intuitive, but not necessarily optimum, test that we have employed involves a normalized ratio of the counts. This scalar test statistic, Λ_d , is given by

$$\Lambda_d = \frac{c_i}{F c_o} - 1. \quad (1)$$

Here F is the ratio of the count rates in the detectors when the probe is viewing a spatially uniform background source. When there is no tumor present, we have expectation values (denoted by $\langle \dots \rangle$) for the data $\langle c_i \rangle = n$ and $\langle c_o \rangle = n/F$ where n is the mean count in the inner detector due to background. In this case $\langle \Lambda_d \rangle = 0$. With a tumor present, the expectation values become $\langle c_i \rangle = s + n$ and $\langle c_o \rangle = n/F$ where s is the mean count increase in the inner detector due to the tumor. We assume that the outer detector count rate is unaffected by the tumor. This assumption is supported by the collimator geometry of the probe (Fig. 1). The expectation value of the test statistic when a tumor is present then becomes $\langle \Lambda_d \rangle = s/n > 0$. Notice this discussion assumes that the signal,

and background, n , are deterministic quantities. However, the dual probe was designed for a task with background variation. Despite this simplification, the dual probe used with the test statistic in Eq. (1) has performed quite well.

With a decision variable for the system, we can form a figure of merit to evaluate different dual-probe designs. Following the recommendations of Swets and Pickett (9) we chose the ROC figure of merit, d_a , given by

$$d_a = \frac{\langle \Lambda_d \rangle_1 - \langle \Lambda_d \rangle_0}{\sqrt{\frac{\sigma_1^2 + \sigma_0^2}{2}}} \quad (2)$$

Here, $\langle \Lambda_d \rangle_1$ and σ_1^2 are the mean and variance of Λ_d given that a tumor is present, and $\langle \Lambda_d \rangle_0$ and σ_0^2 are the mean and variance given that no tumor is present. The expectation values of Λ_d were discussed above. The variances can be calculated from the formula

$$\sigma^2 = \sigma_{c_i}^2 \left[\frac{\partial \Lambda_d}{\partial c_i} \right]^2 + \sigma_{c_o}^2 \left[\frac{\partial \Lambda_d}{\partial c_o} \right]^2 \quad (3)$$

evaluated at $c_i = \langle c_i \rangle$ and $c_o = \langle c_o \rangle$. In this formula, $\sigma_{c_i}^2$ and $\sigma_{c_o}^2$ are variances for c_i and c_o . But, if we disregard background and tumor activity variations as above, c_i and c_o are Poisson random variables. Thus $\sigma_{c_i}^2 = \langle c_i \rangle$ and $\sigma_{c_o}^2 = \langle c_o \rangle$ which gives

$$\sigma^2 = \left[\frac{\langle c_i \rangle}{F \langle c_o \rangle} \right]^2 \left[\frac{1}{\langle c_i \rangle} + \frac{1}{\langle c_o \rangle} \right]. \quad (4)$$

To calculate σ_1^2 and σ_0^2 we substitute the corresponding tumor-present and tumor-absent values of $\langle c_i \rangle$ and $\langle c_o \rangle$ into Eq. (4). If we assume that the signal is small (i.e., $s \ll n$) then we find we find

$$\sigma_1^2 \approx \sigma_0^2 = \frac{1 + F}{n} \quad (5)$$

and

$$d_a = \frac{s}{\sqrt{n(1 + F)}}. \quad (6)$$

We used the figure of merit given in Eq. (6) to optimize the design parameters of the dual probe.

As noted before, the test presented in Eq. (1) is not necessarily optimum. We are investigating a Bayesian test (10) for tumor presence based on models of the probability laws governing tumor and background activities.

ACKNOWLEDGMENTS

The authors thank Rexon Inc. for constructing the NaI(Tl) crystals to our specifications. This work was supported by the National Cancer Institute under Grant PO1 CA 23417.

REFERENCES

1. Hinkle GH, Abdel-Nabi H, Miller EA, et al. Radioimmunodetection of implanted tumors with gamma probe. *NCI Monographs* 1987; 3:83-87.
2. Packer S. Tumor detection with radiopharmaceuticals. *Semin Nucl Med* 1984; 14:21-30.
3. Ubhi CS, Hardy JG, Pegg CAS. Mediastinal parathy-

- roid adenoma: a new method of localization. *Br J Surg* 1984; 71:859-860.
4. Martin DT, Hinkle GH, Tuttle S, et al. Intraoperative radioimmunodetection of colorectal tumor with a hand-held radiation detector. *Am J Surg* 1985; 150:672-675.
 5. Woolfenden JM, Nevin WS, Barber HB, et al. Lung cancer detection using a miniature sodium iodide detector and cobalt-57 bleomycin. *Chest* 1984; 85:84-88.
 6. Reinhardt H, Stula D, Gratzl O. Topographic studies with ^{32}P tumor marker during operations of brain tumors. *Eur Surg Res* 1985; 17:333-340.
 7. Harcke HT, Conway JJ, Tachdjian MO, et al. Scintigraphic localization of bone lesions during surgery. *Skeletal Radiol* 1985; 13:211-216.
 8. Groch MW, Gottlieb S, Mallon SM, et al. A new dual-probe system for the rapid bedside assessment of left ventricular function. *J Nucl Med* 1976; 17:930-936.
 9. Swets JA, Pickett RM. Evaluation of diagnostic systems: methods from signal detection theory. New York: Academic Press, 1982: 29-33.
 10. Melsa JL, Cohn DL. Decision and estimation theory. New York: McGraw-Hill, 1978: 44-47, 60-69.